

400 V in about 30 experiments. Electroporation was indicated by the drop in R_{skin} , and usually occurred before any sensation.

IV. CONCLUSION

The prototype ERD provided *in vitro* transport of SR across the skin due to pulses that cause zero or minimal sensation *in vivo*. Electrical impedance and voltage measurements *in vivo* monitored the ERD-skin contact and showed that sufficient voltage was applied to cause electroporation. Since the distance, d , between the edge of the hole and the surface electrode determines the extent of electric field penetration into viable skin tissue, it is the most crucial parameter for the electrode design. For significant penetration to less than about $50 \mu\text{m}$ d should not exceed $200 \mu\text{m}$. Our results provide additional support for the feasibility of small charged molecule delivery by electroporation.

ACKNOWLEDGMENT

The authors would like to thank T. O. Herndon and T. R. Gowrishankar for advice and discussion.

REFERENCES

- [1] M. R. Prausnitz, S. Mitragotri, and R. Langer, "Current status and future potential of transdermal drug delivery," *Nat. Rev. Drug Discov.*, vol. 3, pp. 115–121, 2004.
- [2] M. R. Prausnitz, V. G. Bose, R. Langer, and J. C. Weaver, "Electroporation of mammalian skin: A mechanism to enhance transdermal drug delivery," *Proc. Nat. Acad. Sci. (USA)*, vol. 90, pp. 10504–10508, 1993.
- [3] U. Pliquet, T. E. Zewert, T. Chen, R. Langer, and J. C. Weaver, "Imaging of fluorescent molecule and small ion transport through human stratum corneum during high-voltage pulsing: Localized transport regions are involved," *Biophys. Chem.*, vol. 58, pp. 185–204, 1996.
- [4] U. Pliquet and M. R. Prausnitz, "Electrical impedance spectroscopy for rapid and non-invasive analysis of skin electroporation," in *Electrically Mediated Delivery of Molecules to Cells: Electrochemotherapy, Electrogenetherapy, and Transdermal Drug Delivery by Electroporation*, M. Jaroszeski, R. Gilbert, and R. Heller, Eds. Totowa, NJ: Humana, 1999, pp. 377–406.
- [5] U. Pliquet and J. C. Weaver, "Electroporation of human skin: Simultaneous measurement of changes in the transport of two fluorescent molecules and in the passive electrical properties," *Bioelectrochem. Bioenerg.*, vol. 39, pp. 1–12, 1996.
- [6] U. Pliquet and C. Gusbeth, "Perturbation of human skin due to application of high voltage," *Bioelectrochem. Bioenerg.*, vol. 51, pp. 41–51, 2000.

Simulation of Biphasic CT Findings in Hepatic Cellular Carcinoma by a Two-Level Physiological Model

Marek Kretowski*, Johanne Bezy-Wendling, and Pierrick Coupe

Abstract—In this paper, we present a two-level physiological model that is able to reflect morphology and function of vascular networks, in clinical images. Our approach results from the combination of a macroscopic model, providing simulation of the growth and pathological modifications of vascular network, and a microvascular model, based on compartmental approach, which simulates blood and contrast medium transfer through capillary walls. The two-level model is applied to generate biphasic computed tomography of hepatocellular carcinoma. A contrast-enhanced sequence of simulated images is acquired, and enhancement curves extracted from normal and tumoral regions are compared to curves obtained from *in vivo* images. The model offers the potential of finding early indicators of disease in clinical vascular images.

Index Terms—Compartment model, computed tomography simulation, enhancement curves, hepatocellular carcinoma, vascular model.

I. INTRODUCTION

Imaging of vascular networks is of major significance for detection and characterization of various pathologies affecting vessels topology, geometry, or function. It allows for detecting early indicators of disease in a non-invasive manner. In this context, models can help to understand the mechanisms underlying image formation, by testing hypotheses concerning pathology origins. It seems obvious that only physiological models can achieve this task [1]. In [2], we proposed an image modeling approach able to represent geometric and haemodynamic properties of vascular networks, down to the macroscopic level of arterioles and venules (around $50\text{--}100 \mu\text{m}$). However, early signs of onset and development of the disease generally arise at finer scales (i.e., capillaries) and vascular modeling should not therefore be restricted to the macroscopic level. This is especially crucial for realistic contrast material propagation, where simplified solutions as proposed in [3] are of limited use.

In this paper, we propose to combine our physiological model with a microscopic compartment one. The originality of this approach lies in the fact that it is neither limited to a purely geometric description as in many macroscopic models (e.g., [4] and [5]), nor to a specifically functional one, like in several studies based on compartment models [6], [7]. The strength of the proposed approach is in the combination of the two main aspects influencing vascular imaging: morphology (vessels) and function (contrast medium propagation). Moreover, this two-level approach offers the possibility to simulate enhancement changes related to focal or diffuse vascular diseases.

The proposed method is applied to simulating of hepatocellular carcinoma (HCC) observed by means of biphasic computed tomography (CT). In hepatic carcinogenesis, tumor evolution expresses itself by important capillarization [8], with arterialization, and decrease in portal supply. Early tumor characterization (benign nodule versus malignant tumor) is fundamental in the therapy choice, and imaging markers of

Manuscript received April 25, 2005; revised December 21, 2005. This work was supported in part by the Bialystok Technical University under Grant W/WI/5/05. Asterisk indicates corresponding author.

*M. Kretowski is with the Faculty of Computer Science, Bialystok Technical University, Wiejska 45a, 15-351, Bialystok, Poland (e-mail: mkret@ii.pb.bialystok.pl).

J. Bezy-Wendling and P. Coupe are with the Laboratoire Traitement du Signal et de l'Image, INSERM U642, Université de Rennes 1, Rennes 35042, France.

Digital Object Identifier 10.1109/TBME.2006.888834

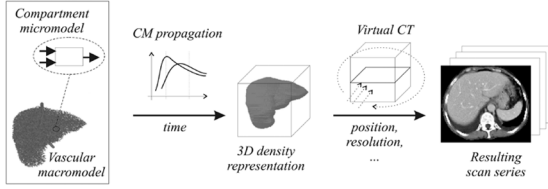


Fig. 1. Framework of the model-based approach to medical images understanding. Two-level vascular model is coupled with virtual CT modality. During the contrast medium propagation at given time instants, density representations are generated and then CT scans are reconstructed based on classical algorithm of filtered back-projections. More details can be found in [2].

malignancy are of crucial importance. Our approach offers the potential to reveal this kind of markers due to the modeling chain going from an organ to time stamped sequences of images (see Fig. 1).

In Section II, the macroscopic and microscopic levels of the model are briefly described and the method of the contrast enhanced CT modeling is also explained. The results are summarized in Section III, and the paper is concluded in the last section.

II. MODEL

A. Macrovascular Model

The model enables us to simulate up to three connected vascular structures. It is especially suitable for the liver, with its two supplying trees [hepatic artery (HA) and portal vein (PV)], and hepatic vein (HV). The organ is composed of macro-functional units (MFUs), made of tissue and small vessels. Several classes of MFUs can co-exist in the organ. Variations of physiological properties (such as blood pressure and flow, or time-dependent mitosis/necrosis rates) allow us to introduce pathological changes. At each growth cycle of the organ, new MFUs appear, and are perfused by new vessels sprouting from the existing network (angiogenesis). A local optimization process is performed to determine new bifurcations geometry, respecting the minimum blood volume criterion. Each binary tree is composed of consecutive vessel segments (rigid tubes with wall thickness depending on their type and radius), characterized by their geometry, blood pressure and flow (governed by Poiseuille law). After perfusion of a new MFU, characteristics of the vascular structures (blood flow, pressure, and radii) are updated [9]. As shown in Fig. 1, an independent microscopic model represents each MFU.

B. Microvascular Model

Compartment models have been applied recently to simulation of vessels/tissue exchanges ([10] and [11]) or to estimation of perfusion and capillary permeability [12]. In contrast to such global models, our approach enables to locally compute the contrast medium concentration. It also takes into account the portal circulation and integrates liquid movements (not only molecular transfer). Moreover, the direct coupling between the microvascular and the macrovascular models allows us to generate not only enhancement curves, but also dynamic enhanced images.

The model entries are the two blood supplies coming from hepatic arteriole (ha), and portal venule (pv). They are characterized by their flows, $Q_{ha}(t)$ and $Q_{pv}(t)$, and contrast medium concentrations, $C_{ha}(t)$ and $C_{pv}(t)$, which are deduced from contrast medium propagation in the macroscopic model. The three compartments of the model are depicted in Fig. 2: “sinusoids,” “extra-cellular space,” and “hepatic venules.” Blood arriving in the sinusoids is mixed with contrast medium at the concentration $C_s(t)$ and goes through the capillary wall into the extra-cellular space with the flow $F(t)$. Plasma

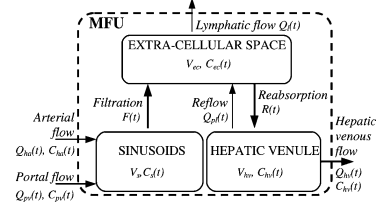


Fig. 2. Three-compartment microscopic model proposed for simulating of hepatic transvascular exchanges.

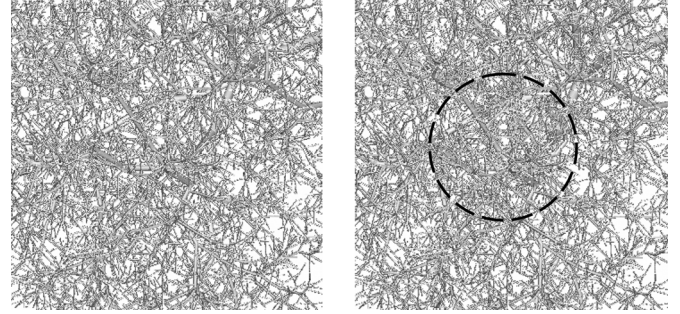


Fig. 3. Simulation of hepatic arterial structure in normal liver (left) and HCC (right, the hyper-vascular tumoral region is denoted by circle).

and contrast medium molecules can exit the extra-cellular space compartment by two possible ways: 1) due to the hydrostatic and osmotic pressures [13] toward hepatic venules, with flow $R(t)$, and 2) toward lymphatic capillaries, with flow $Q_l(t)$. In this compartment, the liquid has the concentration $C_{ec}(t)$. Finally, blood leaves MFU by hepatic venule, with flow $Q_{hv}(t)$. The re-flow $Q_{pl}(t)$ from hepatic venules into extra-cellular space [14] is also integrated into the model. The contrast medium concentration in the third compartment is $C_{hv}(t)$. As the macroscopic vascular model does not currently include the lymphatic circulation, the lymphatic flow from the extra-cellular space ($Q_{pl}(t)$) is artificially connected to the venous circulation ($Q_{hv}(t)$) leading to only one output: the hepatic venous flow. In order to study variations in concentration in the different compartments, we formalized exchanges by the following differential equations:

$$V_s \frac{dC_s(t)}{dt} = C_{ha}(t)Q_{ha}(t) + C_{pv}(t)Q_{pv}(t) - C_s(t)F(t) \quad (1)$$

$$V_{ec} \frac{dC_{ec}(t)}{dt} = C_s(t)F(t) + C_{hv}(t)Q_{pl}(t) - C_{ec}(t)(R(t) + Q_l(t)) \quad (2)$$

$$V_{hv} \frac{dC_{hv}(t)}{dt} = C_{ec}(t)R(t) - C_{hv}(t)(Q_{pl}(t) - Q_{hv}(t)). \quad (3)$$

The compartment volumes (V_s , V_{ec} , V_{hv}) are obtained by dividing the corresponding volumes (sinusoids, extra-cellular, and hepatic vein) of the liver by the number of MFUs constituting it. For transvascular flows, we used general circulation data, leading to the following relations [6]: $F = Q_{ha} + Q_{pv}$, $R = 0.84F$, $Q_l = 0.21F$, and $Q_{pl} = R + Q_l - F$.

Even if the macroscopic model currently sets the same pressure to all MFUs, microvascular blood flows (F , R , and Q_{pl}) depend on hydrostatic and osmotic pressures. The flow evolution with pressures and permeability can be easily integrated by using equations like the one of F [6]: $F = K_s * (P_s - P_{ec} - \pi_{pl} + \pi_i)$, where P_s and P_{ec} are hydrostatic pressure in sinusoids and extra-cellular space, π_{pl} and π_i are corresponding osmotic pressures. Coefficient K_s reflects the capillary permeability.

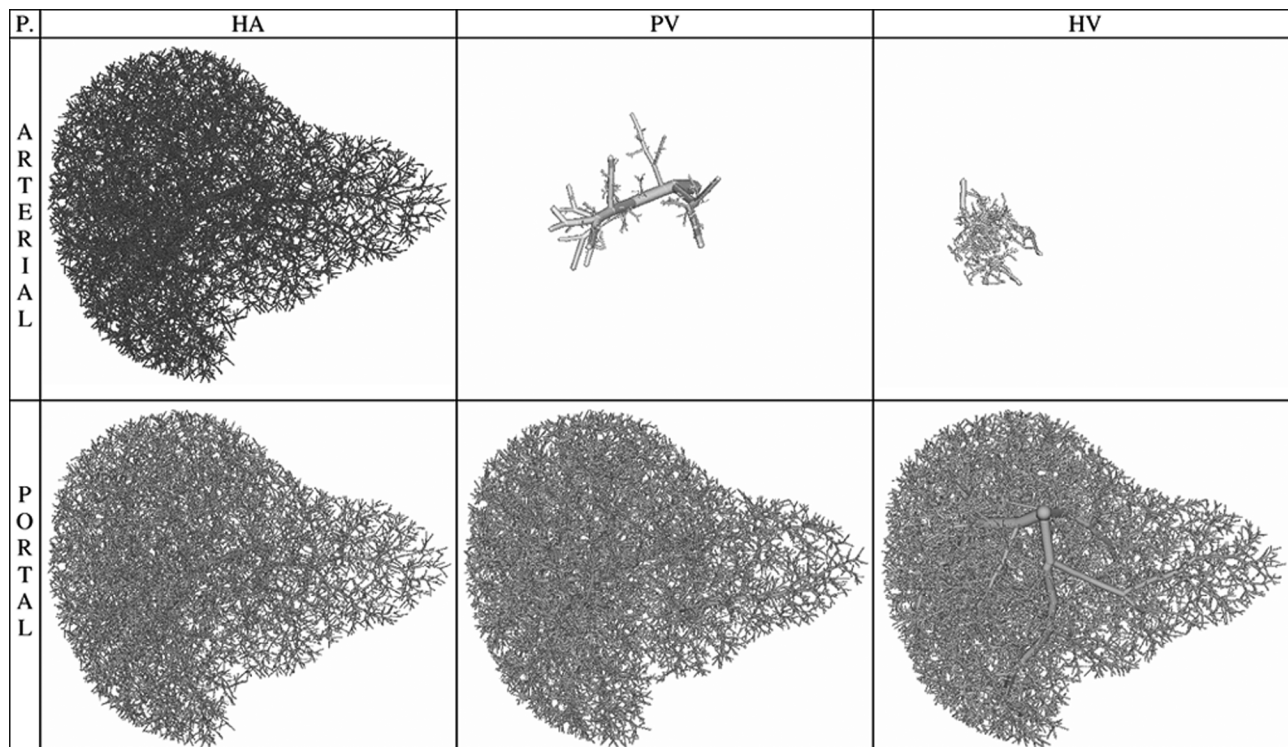


Fig. 4. Simulation of contrast medium propagation (only injected vessels are displayed; gray level corresponds to contrast concentration).

C. Biphasic CT Modeling

The first step to simulate dynamic CT [3] is injection of contrast medium into HA and PV. It propagates through vessels and parenchyma. The concentration of the contrast medium is calculated in all the macroscopic vessels, as well as in each MFU. A 3-D representation is generated, where each voxel is assigned an attenuation coefficient depending on its composition (blood/parenchyma/contrast medium). Then, the CT scan acquisition is carried out through the following steps: 1) X-ray cone beam projections with noise-added are computed using the Radon transform; 2) projections are filtered in the Fourier domain, by a band-limited filter; 3) a back-projection is applied to reconstruct the image. Virtual CT simulation is described in more details in [2]. It should be noticed that in this model of CT acquisition, certain simplifications have been made concerning, e.g., the surrounding anatomical structures that are not present.

III. RESULTS

We applied the proposed two-level model to simulation of biphasic CT of the liver affected by HCC. HCC is the most common hyper-vascular hepatic malignant tumor. The main parameters of the macroscopic model, with some details concerning, among other things, initialization (external organ envelope, initial vessels, ...) and growth simulations can be found in [2] and [3]. Different classes of MFUs are used to simulate normal parenchyma and a focal lesion. Abnormal MFUs are introduced among normal ones, in a bounded area of the organ. Tumoral MFUs co-exist with the healthy ones, and evolve with them, in a succession of regeneration events (mitosis/necrosis). Some parameters of pathological MFUs are modified (e.g., probability of mitosis, maximum local density and blood flow are increased in the pathological case, compared to healthy tissue). Moreover, these MFUs are only supplied by arteriole and not by portal venule [8]. Significantly increased blood flow (4 times compared to normal tissue)

in arterial and absence of portal supply constitute differences between normal liver and HCC simulated at the microscopic level.

Profiles used for contrast medium injection are taken from [11]. Compartments volumes are adapted to the volume of the MFU (total hepatic volume divided by the number of MFUs, which is around 12000 at the end of the organ growth): $V_s = 57 \text{ ml}/12000$, $V_{ec} = 524 \text{ ml}/12000$, $V_{hv} = 15 \text{ ml}/12000$ [15].

Fig. 3 shows simulated vessels of HA, in two regions: normal and HCC. Tumor arterialization of nodules and HCC can be observed. Fig. 4 shows three simulated vascular trees displayed at two acquisition times, typically used in clinical examinations: 1) arterial phase (20–30 s after injection), when the iodinated X-ray dye is mainly in HA, not in PV and arrives in HV only in the tumor, and 2) portal phase, when a large amount of dye arrives in the portal tree. This 3-D visualization allows us to isolate the lesion during the arterial phase and confirms its significance for hypervascular tumor characterization. In Fig. 5(a), simulated CT scans (slice thickness—5 mm, pixel size 0.125 mm, 8-bit gray levels, ...) of the same trees as in Fig. 4 are presented. As expected, HCC is hyper-intense in the first phase, due to the large contrast concentration in HA (an artery pointed by white arrows). During the second phase, the lesion conspicuity decreases significantly. This can be explained by an increase of normal parenchyma enhancement, resulting from contrast supplied by portal vein (strongly injected portal vein pointed by black arrow). In Fig. 5(b), simulations of CT findings concerning a few times smaller tumor placed at the same location are presented. It can be noticed that the tumor conspicuity evolves overtime in analogous way and the lesion is still visually detectable in arterial phase. However, when the arterial supply is decreased for HCC (50% of the previous blood flow), the lesion becomes not visible even in HA [Fig. 5(c)].

The direct comparison of the simulated CT scans with the real data is not an easy task, because, except for CT images, we usually have only partial knowledge about the pathological changes for a given patient.

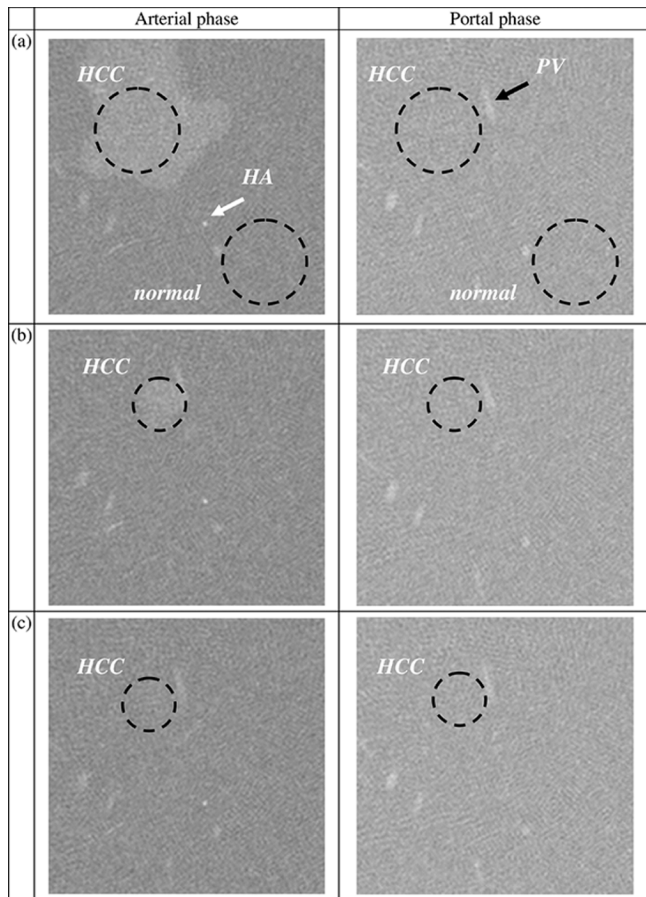


Fig. 5. Simulated biphasic CT scans (slice thickness—5 mm, pixel size 0.125 mm, 8-bit gray levels,...): (a) extensive lesion—HCC, (b) smaller tumor, and (c) the same lesion as in (b) but with decreased arterial supply.

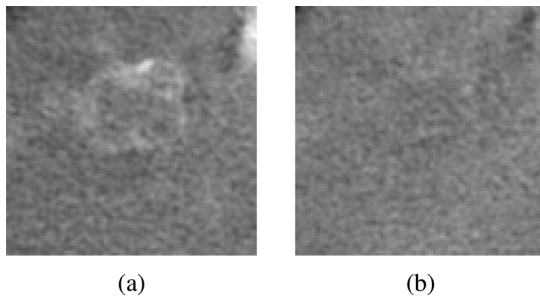


Fig. 6. Real CT slices with confirmed diagnosis of HCC in (a) arterial and (b) portal phase.

In clinical conditions, structural and functional characteristics of the lesion are obviously inaccessible. In Fig. 6, typical HCC patterns in two standard phases are presented. We observed that the general agreement is satisfactory, however the real tumor is more heterogeneous (maybe due to necrosis in the center).

Finally, the enhancement curves computed in normal parenchyma and tumor are represented in Fig. 7. They have been obtained using a representative set of physiological and physical parameters. Then these simulated curves have been compared with those measured by Kim *et al.* on 24 patients [11]. We would like to stress that we obtained a good agreement between simulated and real enhancement curves. Influence of parameters will be evaluated in future works.

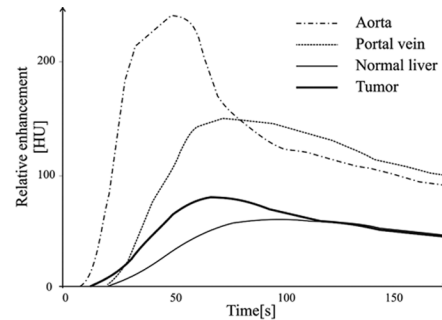


Fig. 7. Enhancement curves derived from normal and tumoral ROIs depicted in Fig. 5(a).

IV. CONCLUSION

In this paper, we proposed a two-level physiological model combining macroscopic and microscopic vascular properties. The model enables to relate first signs of microvascular pathological alterations to changes in clinical images. The proposed approach is exemplified by simulation of biphasic CT of HCC and the impact of certain tumor characteristics (i.e., tumor size and arterial supply) on the lesion conspicuity is studied. Visual patterns and enhancement curves derived from simulated scans are in good agreement with real data, however this tentative validation has to be extended. This study demonstrates that the model-based method constitutes a good way toward a better interpretation of clinical images and could be useful in finding early image indicators of a disease, like measurable vascular changes corresponding to the development of HCC.

It is natural that presented models can be extended in many directions. For example, in the compartment model, a direct communication between the sinusoids and the hepatic venules can be incorporated and additional functional parameters can be introduced, like the capillaries permeability (via pore sizes and number or the basal membrane structure). The macro-vascular model can profit from more elastic vessels representation (e.g., based on Bezier curves). Moreover, the simplified cone beam scanning can be replaced by multislice acquisitions.

ACKNOWLEDGMENT

The authors would like to thank Prof. J.-L. Coatrieux for his support and inspiring discussions.

REFERENCES

- [1] J. Demongeot, J. Bezy-Wendling, J. Mattes, P. Haigron, N. Glade, and J. Coatrieux, "Multiscale modeling and imaging: The challenges of bio-complexity," *Proc. IEEE*, vol. 91, pp. 1723–1737, Oct. 2003.
- [2] M. Kretowski, Y. Rolland, J. Bezy-Wendling, and J. Coatrieux, "Physiologically based modeling of 3-D vascular networks and CT-scan angiography," *IEEE Trans. Med. Imag.*, vol. 22, no. 2, pp. 248–257, Feb. 2003.
- [3] J. Bezy-Wendling, M. Kretowski, and Y. Rolland, "Hepatic tumor enhancement in CT: Combined models of liver perfusion and dynamic imaging," *Comput. Biol. Med.*, vol. 33, pp. 77–89, 2003.
- [4] M. Zamir, "Arterial branching within the confines of fractal L-system formalism," *J. Gen. Physiol.*, vol. 118, pp. 267–275, 2001.
- [5] J. Bezy-Wendling, M. Kretowski, Y. Rolland, and W. L. Bidon, "Toward a better understanding of texture in vascular CT scan simulated image," *IEEE Trans. Biomed. Eng.*, vol. 48, no. 1, pp. 120–124, Jan. 2001.
- [6] J. Bert and K. Pinder, "Analog simulation of the human microvascular exchange system," *Simulation*, vol. 39, pp. 89–95, 1982.
- [7] R. Materne *et al.*, "Non-invasive quantification of liver perfusion with dynamic CT and a dual input one-compartmental model," *Clin. Sci.*, vol. 99, pp. 517–525, 2000.
- [8] S. Efremidis and P. Hytiroglou, "The multistep process of hepatocarcinogenesis in cirrhosis with imaging correlation," *Eur. Radiol.*, vol. 12, pp. 753–764, 2002.

- [9] M. Kretowski, Y. Rolland, J. Bezy-Wendling, and J. Coatrieux, "Fast algorithm for 3-D vascular tree modeling," *Comput. Meth. Prog. Biol.*, vol. 70, no. 2, pp. 129–136, 2003.
- [10] K. Bae, J. Heiken, and J. Brink, "Aortic and hepatic contrast medium enhancement at CT, prediction with a computer model," *Radiology*, vol. 207, pp. 647–655, 1998.
- [11] S. Kim, J. Kim, J. Han, K. Lee, and B. Min, "Prediction of optimal injection protocol for tumor detection in contrast-enhanced dynamic hepatic CT using simulation of lesion to liver contrast difference," *Comput. Med. Imag. Graphics*, vol. 24, pp. 317–327, 2000.
- [12] G. Brix *et al.*, "Regional blood flow, capillary permeability, and compartmental volumes: Measurement with dynamic CT—Initial experience," *Radiology*, vol. 210, pp. 269–276, 1999.
- [13] E. Carson and C. Cobelli, *Modelling Methodology for Physiology and Medicine*. New York: Academic, 2001.
- [14] C. Chapple *et al.*, "A model of human microvascular exchange: Parameter estimation based on normals and nephrotics," *Comput. Meth. Prog. Biol.*, vol. 41, pp. 33–54, 1993.
- [15] B. Fagrell, "Advances in microcirculation network evaluation: An update," *J. Microcirc.*, vol. 15, pp. 34–40, 1995.

Cancellation of Ventricular Activity in the ECG: Evaluation of Novel and Existing Methods

Mathieu Lemay*, Jean-Marc Vesin, Adriaan van Oosterom, Vincent Jacquemet, and Lukas Kappenberger

Abstract—Due to the much higher amplitude of the electrical activity of the ventricles in the surface electrocardiogram (ECG), its cancellation is crucial for the analysis and characterization of atrial fibrillation. In this paper, two different methods are proposed for this cancellation. The first one is an average beat subtraction type of method. Two sets of templates are created: one set for the ventricular depolarization waves and one for the ventricular repolarization waves. Next, spatial optimization (rotation and amplitude scaling) is applied to the QRS templates. The second method is a single beat method that cancels the ventricular involvement in each cardiac cycle in an independent manner. The estimation and cancellation of the ventricular repolarization is based on the concept of dominant T and U waves. Subsequently, the atrial activities during the ventricular depolarization intervals are estimated by a weighted sum of sinusoids observed in the cleaned up segments. ECG signals generated by a biophysical model as well as clinical ECG signals are used to evaluate the performance of the proposed methods in comparison to two standard ABS-based methods.

Index Terms—Atrial fibrillation, average beat subtraction, ECG preprocessing, QRST cancellation.

I. INTRODUCTION

Atrial fibrillation (AF) is the most common type of human cardiac arrhythmia. The diagnosis of AF as such has been based mainly on

Manuscript received February 13, 2006; revised August 20, 2006. This work was supported in part by the Theo-Rossi-Di-Montelera Foundation and in part by the Swiss National Science Foundation (SNSF). *Asterisk indicates corresponding author.*

*M. Lemay is with Ecole Polytechnique Fédérale de Lausanne (EPFL), Signal Processing Institute, Lausanne CH-1015, Switzerland. (e-mail: mathieu.lemay@epfl.ch).

J.-M. Vesin and V. Jacquemet are with the Ecole Polytechnique Fédérale de Lausanne (EPFL), Signal Processing Institute, Lausanne CH-1015, Switzerland.

A. van Oosterom, and is with the Department of Cardiology, CHUV, Lausanne CH-1015, Switzerland.

L. Kappenberger is with Cardiomet, CHUV, Lausanne CH-1015, Switzerland.

Digital Object Identifier 10.1109/TBME.2006.888835

visual inspection of the surface electrocardiogram (ECG) [1]. Due to the much higher amplitude of the electrical ventricular activity (VA) on the surface ECG, cancellation of the ventricular involvement is crucial in the study of AF on ECGs. Two approaches are generally used to perform this task: source separation algorithms and matched template subtraction. Source separation algorithms try to find uncorrelated components using a principal component analysis (PCA), or to find independent components in an instantaneous linear mixture using an independent component analysis (ICA). PCA have previously been employed to monitor the effects of drugs [2] and assess the effects of linear left atrial ablation [3]. ICA has been applied in order to obtain ECG signals devoid of VA involvement [4] and [5]. In these algorithms, even if the obtained components do not seem to contain any VA involvement, they are not anymore associated to specific locations on the thorax.

Other well-known methods are based on the subtraction of matched templates. These methods assume that, in the same patient, ventricular complexes generally exhibit a limited number of forms. An average (template) of these distinct complexes is then used to subtract the VA. In this paper, the standard average beat subtraction (ABS) method (without any features) is labelled as ABS_1 . Studies of noninvasive assessment of the atrial cycle length [6], frequency analysis of AF and drugs effects [7] and classification of paroxysmal and persistent AF [8] are some of the numerous examples in which matching template and subtraction methods were used to cancel ventricular involvement. A refined method was described by Stridh and Sörnmo [9], labelled here as ABS_2 . In their method, two major features are added: F wave reduction and spatiotemporal alignment. In this method, several beats for each morphology are needed to create the templates. In clinical practice, the standard ECG consists of 10-s recordings, and high quality templates may be difficult to create.

In this paper, we propose two methods for ventricular wave suppression. The first one is a further refinement of ABS_1 , labelled as ABS_3 , and as such can be applied only if a sufficiently long episode of AF in the ECG signal is available. The second is a method that permits cancellation of the ventricular involvement in short episodes of AF in the ECG signal, with a minimum length of one complete cardiac cycle. This method is labelled as single beat (SB). Both the ABS_3 and the SB treat the ventricular depolarization (QRS complexes) and repolarization (T and U waves) separately. A dedicated preprocessing procedure is presented in Section II. The two main steps of ABS_3 are explained in Section III: QRS complex cancellation using templates (Section III-A) and T and U wave cancellation using templates (Section III-B). The two main steps of the SB method are presented in Section IV: cancellation during the JQ intervals using dominant T and U wave approach (Section IV-A) and estimation of AA during the QRS intervals using a weighted sum of sinusoids (Section IV-B). The performances of the two methods are studied in their application to ECG signals generated by a biophysical model of the atria, as well as to clinical recordings (see Section V). By using the model, realistic separate contributions of the atria and the ventricles became available for testing the methods. The performances of the two methods are compared to those of the standard ABS method without (ABS_1) and with (ABS_2) spatiotemporal alignment, as was proposed in [9].

II. PREPROCESSING

In the standard 12-lead ECG, only two of the first six leads (I, II, III, VR, VL, and VF) are linearly independent. This justified the expression of the pertinent information by an T -by-8 matrix \mathbf{X} that comprises T samples from eight leads: two limb leads (VR and VL) and six precordial leads (V1 to V6). A derivative-based method was applied to the root mean square (rms) signal to detect ventricular complexes [10]. In the i th